Edelweiss Applied Science and Technology
ISSN: 2576-8484
Vol. 7, No. 1, 38-70
2023
Publisher: Learning Gate
DOI: 10.55214/25768484.v7i1.333

Analytical study regarding the topological optimization of an automotive gear wheel pair

Mihai Gaidur[1], Ionut Pascal[1]*, Edward Rakosi[1], Tudor-Marian Ulian[1], Gheorghe Manolache[1]
[1]"Gheorghe Asachi" Technical University of Iași, Faculty of Mechanical Engineering, Str. Prof. Dr. Doc. Dimitrie Mangeron, No 43, 700050 Iasi, Romania; mihai.gaidur@gmail.com (M.G); ionut.pascal@yahoo.com (I.P); edward.rakosi@academic.tuiasi.ro (E.R); tudor-marian.ulian@academic.tuiasi.ro (T.U); gheorghe.manolache@academic.tuiasi.ro (G.M).

Abstract: This academic research explores the application of topology optimization to enhance the design of an automotive gearwheel pair. The study establishes boundary and load conditions, conducting finite element simulations to assess the impact on the gear pair's performance. The primary objective is to reduce component volume while maintaining the initial rigidity of the gear pair. The study uses scenario-based topology optimization to change the percentages of mass reductions and then looks at how these changes affect things like the safety factor, Von Mises stress, displacement, and equivalent strain. The study highlights the trade-offs between mass reduction and the gear pair's mechanical performance, emphasizing the need for a comprehensive risk/gain analysis in optimization decisions. Various scenarios are presented, with scenario II showing the most favorable outcomes, significantly improving all analyzed parameters for gear z_8. Conversely, scenario V for gear z_9 exhibits a decline in all parameters, making it the least favorable scenario. The study underscores the potential benefits of topology optimization, such as achieving lightweight and durable gear designs, though it acknowledges computational intensity and time constraints. Ultimately, the authors recommend further exploration and optimization based on scenarios III and VI, which exhibit the highest relevance according to the study's results. The research contributes to the broader field of engineering design optimization, with implications for improved automotive transmission systems and drivetrain efficiency.

Keywords: *Additive manufacturing, Automotive gearbox, Automotive transmission system, Finite element simulation, Rigidity preservation, Topology optimisation, Volume reduction.*

1. Introduction

Topology optimisation is a design method that involves finding the optimal layout of a structure or component, given certain design constraints and load requirements. In the case of an automotive gear wheel pair, topology optimisation could be used to identify the most efficient configuration of the gear material to improve its performance. One way to approach topology optimisation of a gear wheel pair is to first define the design constraints and load requirements. For example, the gears must be able to fit within a certain size envelope and be able to withstand the forces generated during operation. The next step is to create a finite element model of the gears, which can be used to simulate how the gears will behave under different loading conditions.

Once the finite element model has been created, topology optimisation algorithms can be used to identify the optimal layout of the gear material. These algorithms work by iteratively removing and adding material to the gears until the optimal configuration is found. The goal is to find a layout that is strong enough to meet the design constraints and load requirements, but also as lightweight as possible to reduce the gear pair's overall mass. Several different topology optimisation algorithms can be used to

History: Received: 12 June 2023; Revised: 25 August 2023; Accepted: 28 September 2023; Published: 10 November 2023
* Correspondence: ionut.pascal@yahoo.com

optimise the design of a gear wheel pair. Some of the most common algorithms include the SIMP (Solid Isotropic Material with Penalization) method, the density-based method, and the genetic algorithm. Each of these algorithms has its strengths and weaknesses, and the best choice will depend on the specific design requirements and constraints of the gears. It is important to mention that the finite element simulations were conducted using a software solution called *Fusion 360*, software that was provided by *AUTODESK Group* with an educational licence. The gears were discretized with a triangular mesh type to attain high degrees of accuracy and effectiveness. This method made it possible to accurately analyse how the gears behaved mechanically under various loading scenarios.

In this study, the effect of topological optimisation on a pair of gears used in a vehicle transmission was examined. The necessary dimensions were determined by following the piston design guidelines. Then, the finite element method was used to analyse the gears and establish reference values as comparison data for the optimisation analyses. After determining the gear's response to mechanical stresses, topological optimisation was conducted, aiming to reduce up to 5% of the initial part volume. The resulting parts were reanalysed using the finite element method to validate the new geometries and compare them to the reference values from the initial analysis [1-7].

2. Load Case Scenario

For the gear loading condition, the following boundary conditions were considered:

2.1. Structural Constraints

Both gears were subjected to fixed-type constraints on their fixing geometries. The degrees of freedom of the gears' position and orientation relative to the shaft are constrained by applying a fixed-type constraint to the relevant geometry that comes into contact with the shaft, which restricts its movement and rotation in all directions except relative to the axis of the shaft. The position and orientation of the gears are thus set with regard to the shaft, ensuring that they remain in that position and orientation throughout the simulation and that any movement or deformation under loading conditions is purely attributable to their mechanical characteristics [8-14].

2.2. Loading Constraints

The applied forces were determined with the help of common design standards [15]. As shown in Figure 1, the gears will experience one tangential load, named F_T, corresponding to their transmission ratios, i_4 and i_5, respectively. The material used for the finite element analysis was case-hardened steel, specifically AISI (American Iron and Steel Institute) 4340 350C QT (Quenched and Tempered) or, as known in DIN standard (Deutsches Institut für Normung),34CrNiMo6 alloy, which has a yield strength, $R_{p0.2}$,of 1178 [MPa], and an ultimate strength, R_m, of 1240 [MPa] [16].

With the help of Figure 2 and Figure 3, the geometries with the applied mesh network were depicted.

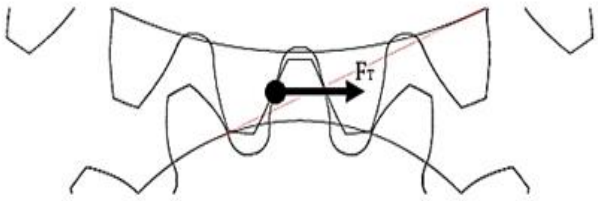

Figure 1.
Graphical depiction of the tangential force distribution during engagement.

Edelweiss Applied Science and Technology
ISSN: 2576-8484
Vol. 7, No. 1: 38-70, 2023
DOI: 10.55214/25768484.v7i1.333

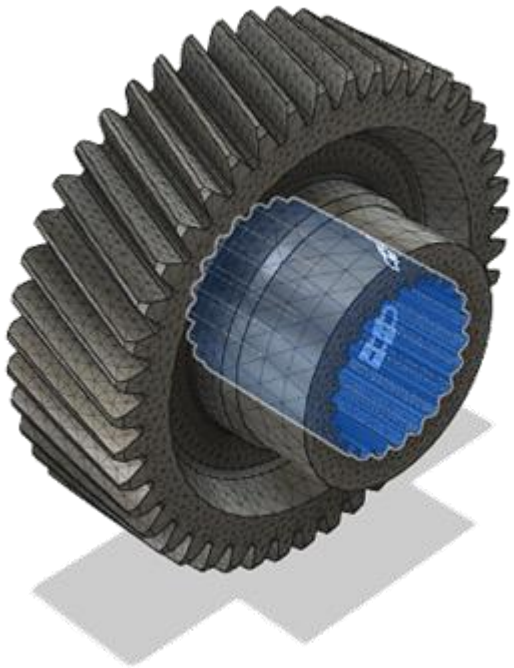

Figure 2.
Isometric view of the gear z_9, with applied mesh. Mounting geometry is highlighted in blue.

Figure 3.
Isometric view of the gear z_8, with applied mesh. Mounting geometry is highlighted in blue.

Edelweiss Applied Science and Technology
ISSN: 2576-8484
Vol. 7, No. 1: 38-70, 2023
DOI: 10.55214/25768484.v7i1.333

3. Load Case Simulation

The results of the simulations were compiled in Table 1, and the graphical representations of the analysed parameters were depicted in Figure 4, Figure 5, Figure 6, Figure 7, Figure 8, Figure 9, Figure 10, and Figure 11.

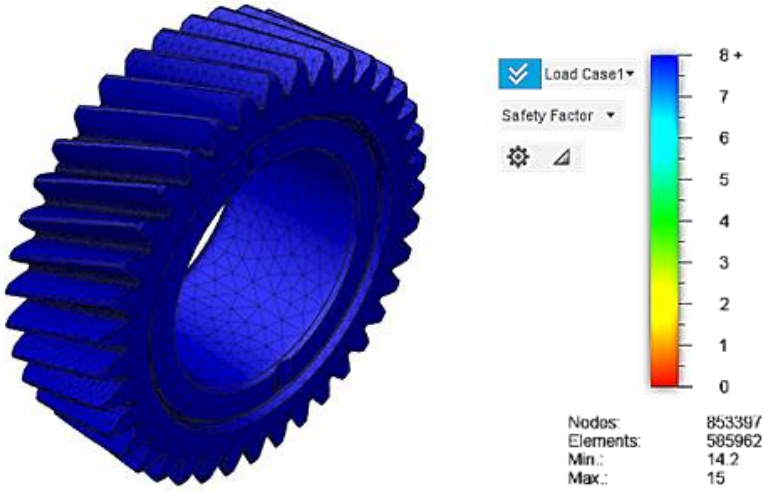

Figure 4.
Minimum safety factor, valid for gear z_8.

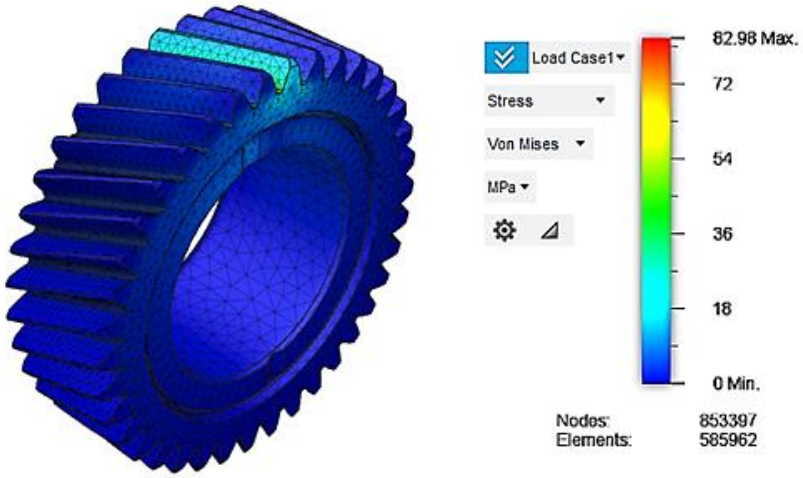

Figure 5.
Maximum Von Mises stress, valid for gear z_8.

Edelweiss Applied Science and Technology
ISSN: 2576-8484
Vol. 7, No. 1: 38-70, 2023
DOI: 10.55214/25768484.v7i1.333

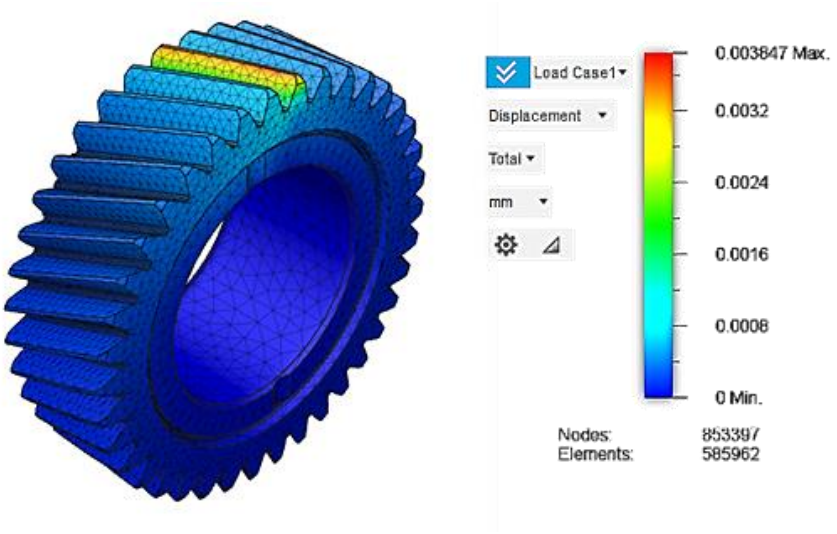

Figure 6.
Maximum displacement, valid for gear z_8.

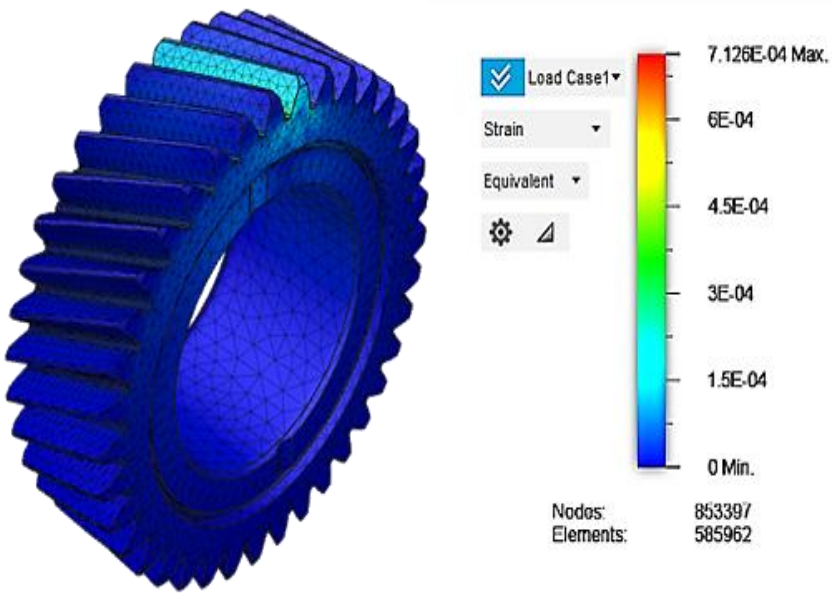

Figure 7.
Maximum equivalent strain, valid for gear z_8.

Edelweiss Applied Science and Technology
ISSN: 2576-8484
Vol. 7, No. 1: 38-70, 2023
DOI: 10.55214/25768484.v7i1.333

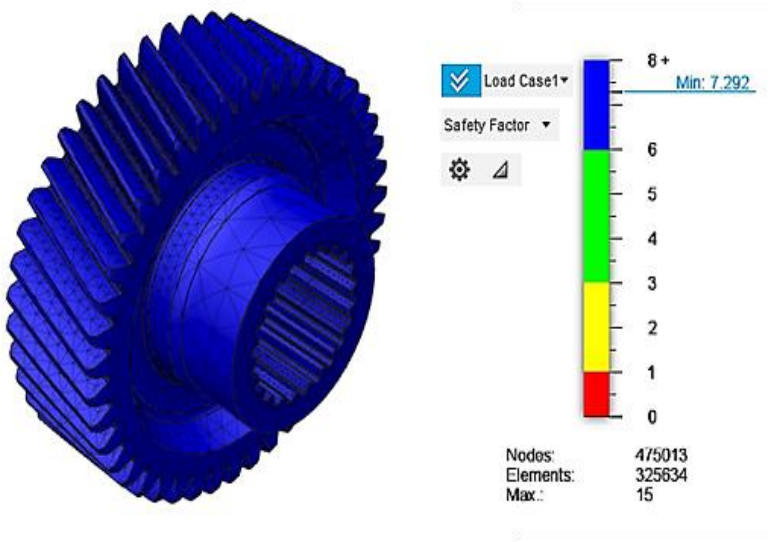

Figure 8.
Minimum safety factor, valid for gear z_9.

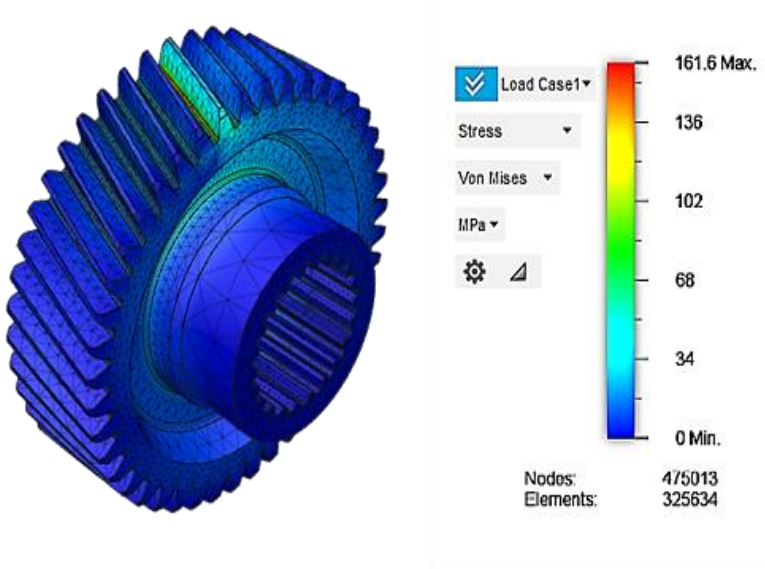

Figure 9.
Maximum Von Mises stress, valid for gear z_9.

Edelweiss Applied Science and Technology
ISSN: 2576-8484
Vol. 7, No. 1: 38-70, 2023
DOI: 10.55214/25768484.v7i1.333

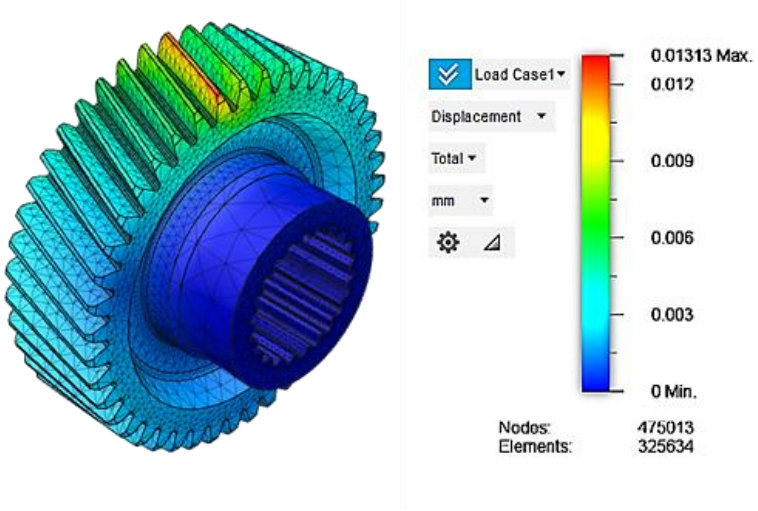

Figure 10.
Maximum displacement, valid for gear z_9.

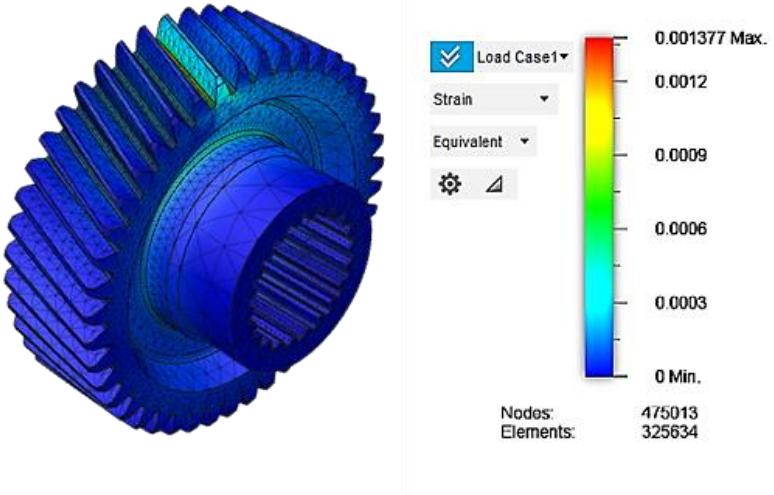

Figure 11.
Maximum equivalent strain, valid for gear z_9.

Table 1.
Results of simulation.

Gear id.	Minimum safety factor	Maximum Von Mises stress [MPa]	Maximum displacement [mm]	Maximum equivalent strain
z_8	14.26	82.6	3.94·10^(-3)	6.3·10^(-4)
z_9	7.52	161.6	1.31·10^(-2)	1.37·10^(-3)

4. Topology Optimization of the Gears

The optimization results, valid for both geared wheels, are displayed in Figure 12, Figure 13, Figure 14, Figure 15, Figure 16, and Figure 17.

Edelweiss Applied Science and Technology
ISSN: 2576-8484
Vol. 7, No. 1: 38-70, 2023
DOI: 10.55214/25768484.v7i1.333

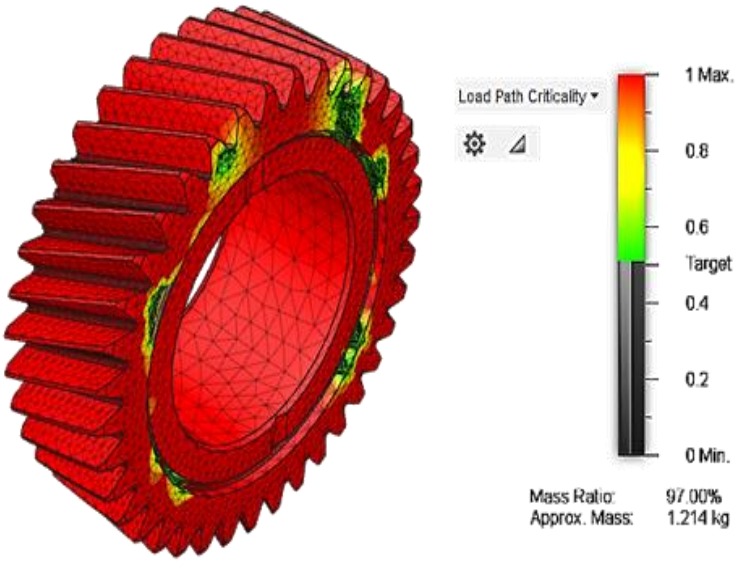

Figure 12.
Representation of the 3% mass reduced gear z_8.

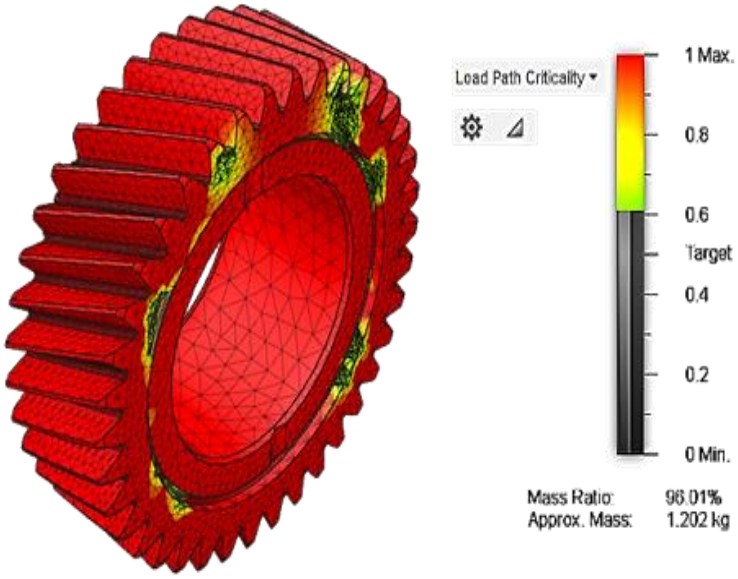

Figure 13.
Representation of the 4% mass reduced gear z_8.

Edelweiss Applied Science and Technology
ISSN: 2576-8484
Vol. 7, No. 1: 38-70, 2023
DOI: 10.55214/25768484.v7i1.333

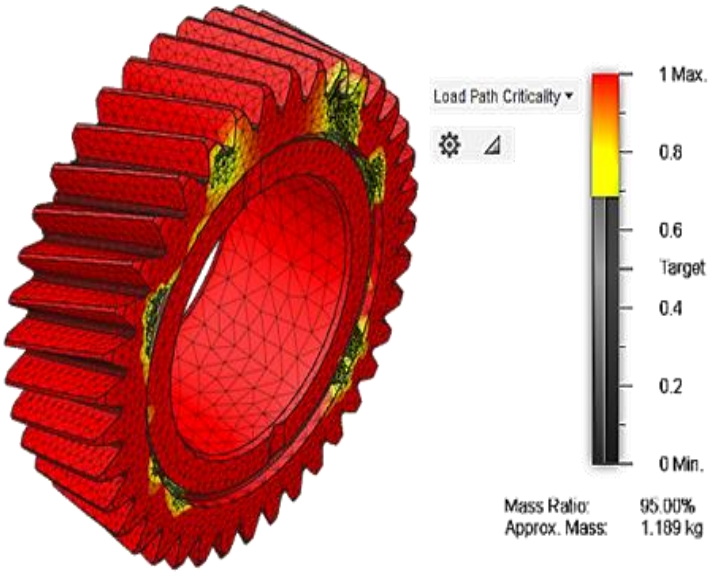

Figure 14.
Representation of the 5% mass reduced gear z_8.

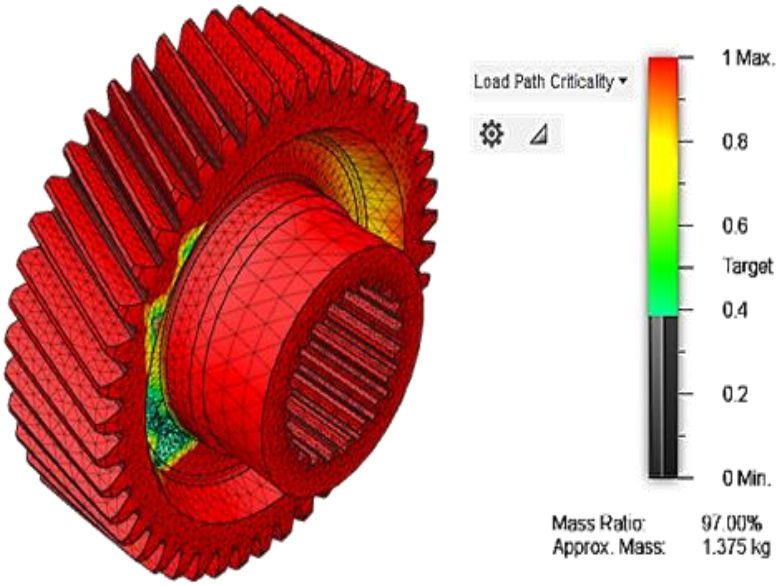

Figure 15.
Representation of the 3% mass reduced gear z_9.

Edelweiss Applied Science and Technology
ISSN: 2576-8484
Vol. 7, No. 1: 38-70, 2023
DOI: 10.55214/25768484.v7i1.333

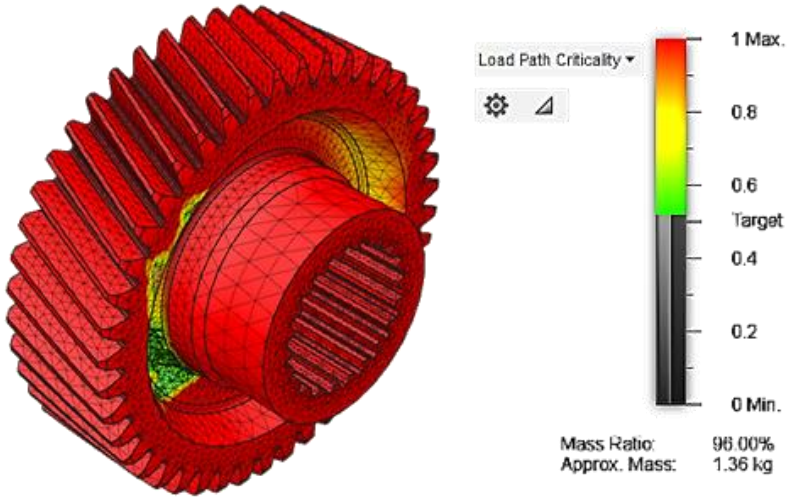

Figure 16.
Representation of the 4% mass reduced gear z_9.

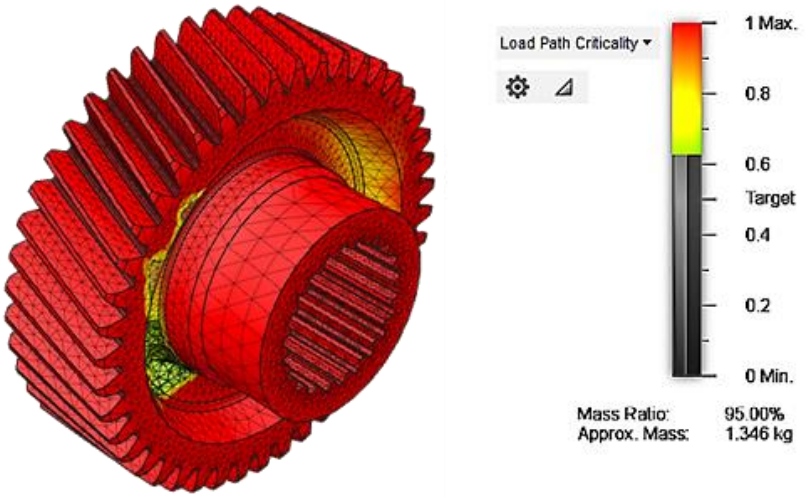

Figure 17.
Representation of the 5% mass reduced gear z_9.

The impact of each optimisation, regardless of the mass reduction percentage, was analysed and compiled in Table 2. Additionally, the percentage variation from the nominal values of each analysed parameter was examined and summarized in Table 3. The green colour indicates an improvement in the performance of the parameter in the corresponding column, while the red colour signifies a decrease in the parameter's performance. The results of the mechanical simulations of the modified geometries are displayed with the help of Figure 18, Figure 19, Figure 20, Figure 21, Figure 22, Figure 23, Figure 24, Figure 25, Figure 26, Figure 27, Figure 28, Figure 29, Figure 30, Figure 31, Figure 32, Figure 33, Figure 34, Figure 35, Figure 36, Figure 37, Figure 38, Figure 39, Figure 40, and Figure 41.

Edelweiss Applied Science and Technology
ISSN: 2576-8484
Vol. 7, No. 1: 38-70, 2023
DOI: 10.55214/25768484.v7i1.333

Table 2.
Impact of optimization.

Gear id.	Mass reduction [%]	Minimum safety factor	Maximum Von Mises stress [MPa]	Maximum displacement [mm]	Maximum equivalent strain
z_8	(Scenario I) 3%	13.45	87.57	4.21·10^(-3)	7.34·10^(-4)
	(Scenario II) 4%	14.4	81.79	3.8·10^(-3)	6.95·10^(-4)
	(Scenario III) 5%	14.26	82.61	3.95·10^(-3)	6.31·10^(-4)
z_9	(Scenario IV) 3%	7.253	162.4	1.43·10^(-2)	1.37·10^(-3)
	(Scenario V) 4%	7.177	164.1	1.53·10^(-2)	1.38·10^(-3)
	(Scenario VI) 5%	7.529	156.5	1.76·10^(-2)	1.26·10^(-3)

Table 3.
Variation from the nominal values of each analysed parameter.

Gear id.	Mass reduction [%]	Minimum safety factor	Maximum Von Mises stress [MPa]	Maximum displacement [mm]	Maximum equivalent strain
z_8	(Scenario I) 3%	-5.28%▼	5.53%▲	9.41%▲	3.07%▲
	(Scenario II) 4%	1.41%▲	-1.43%▼	-1.22%▼	-2.40%▼
	(Scenario III) 5%	0.42%▲	-0.45%▼	2.63%▲	-11.32%▼
z_9	(Scenario IV) 3%	-0.53%▼	0.50%▲	8.91%▲	-0.22%▼
	(Scenario V) 4%	-1.58%▼	1.55%▲	16.53%▲	0.80%▲
	(Scenario VI) 5%	3.25%▲	-3.16%▼	34.20%▲	-8.57%▼

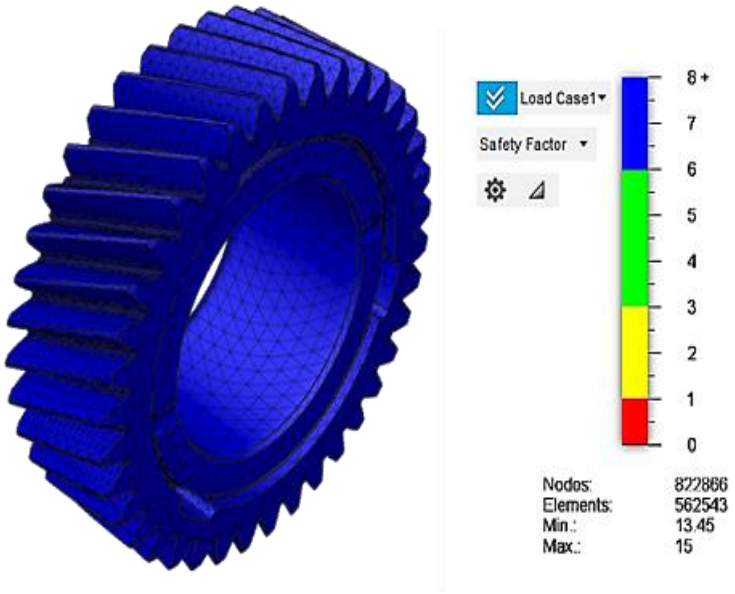

Figure 18.
Minimum safety factor, valid for gear z_8, mass reduced by 3%.

Edelweiss Applied Science and Technology
ISSN: 2576-8484
Vol. 7, No. 1: 38-70, 2023
DOI: 10.55214/25768484.v7i1.333

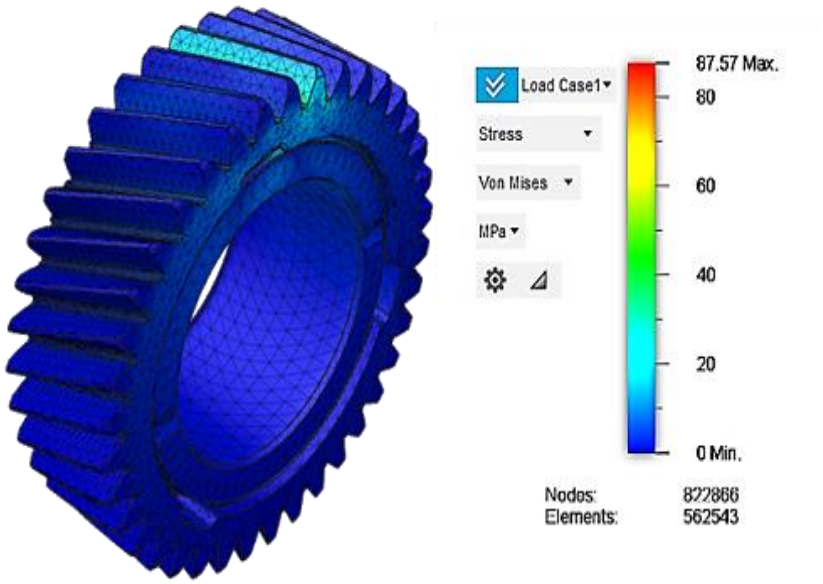

Figure 19.
Maximum Von Mises stress, valid for gear z_8, mass reduced by 3%.

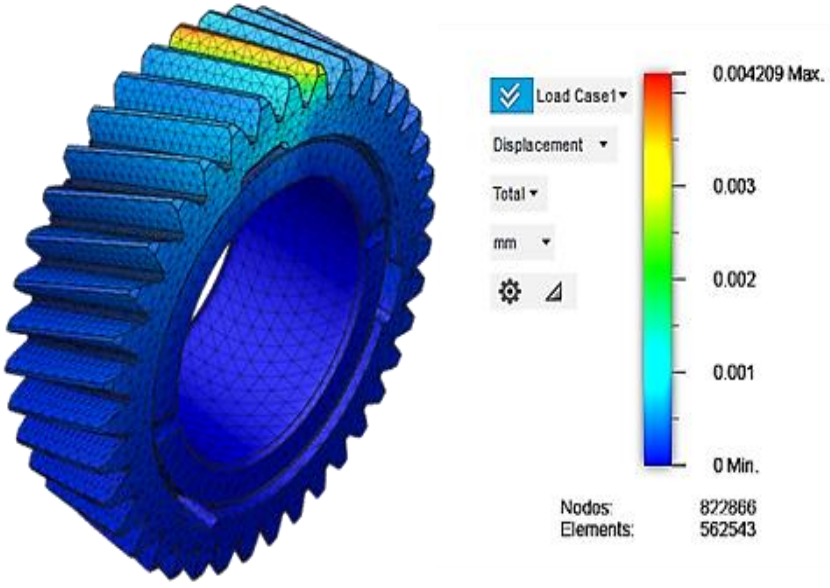

Figure 20.
Maximum displacement, valid for gear z_8, mass reduced by 3%.

Edelweiss Applied Science and Technology
ISSN: 2576-8484
Vol. 7, No. 1: 38-70, 2023
DOI: 10.55214/25768484.v7i1.333

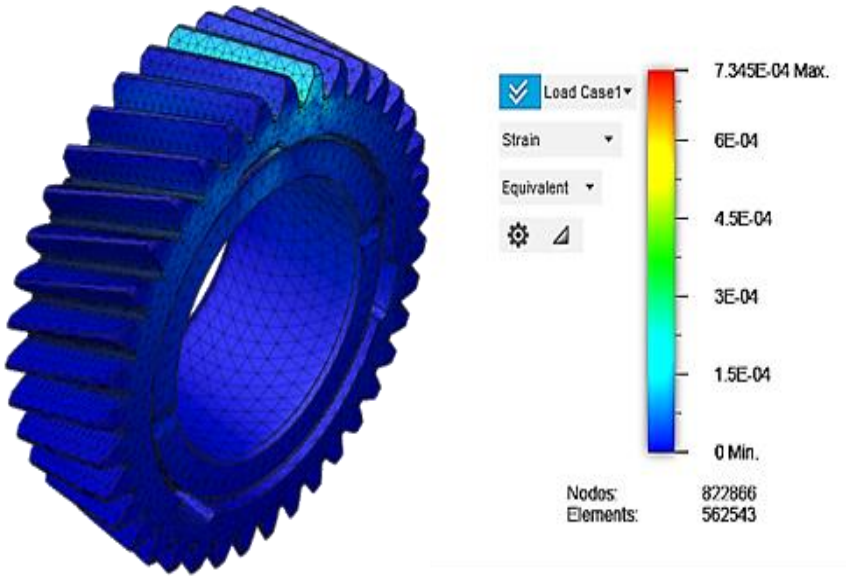

Figure 21.
Maximum equivalent strain, valid for gear z_8, mass reduced by 3%.

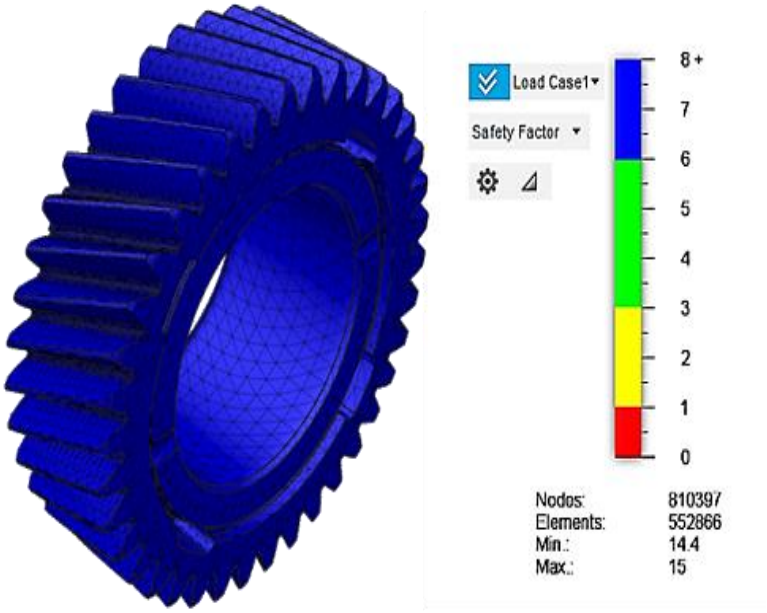

Figure 22.
Minimum safety factor, valid for gear z_8, mass reduced by 4%.

Edelweiss Applied Science and Technology
ISSN: 2576-8484
Vol. 7, No. 1: 38-70, 2023
DOI: 10.55214/25768484.v7i1.333

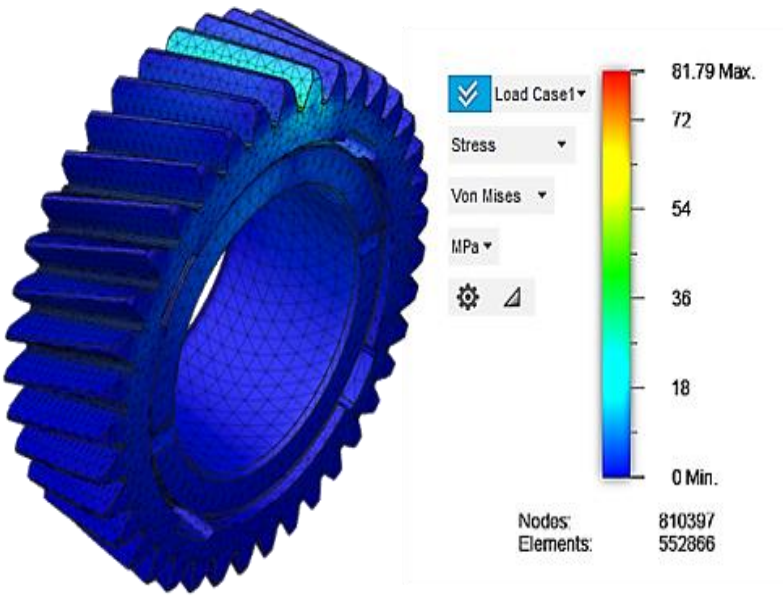

Figure 23.
Maximum Von Mises stress, valid for gear z_8, mass reduced by 4%.

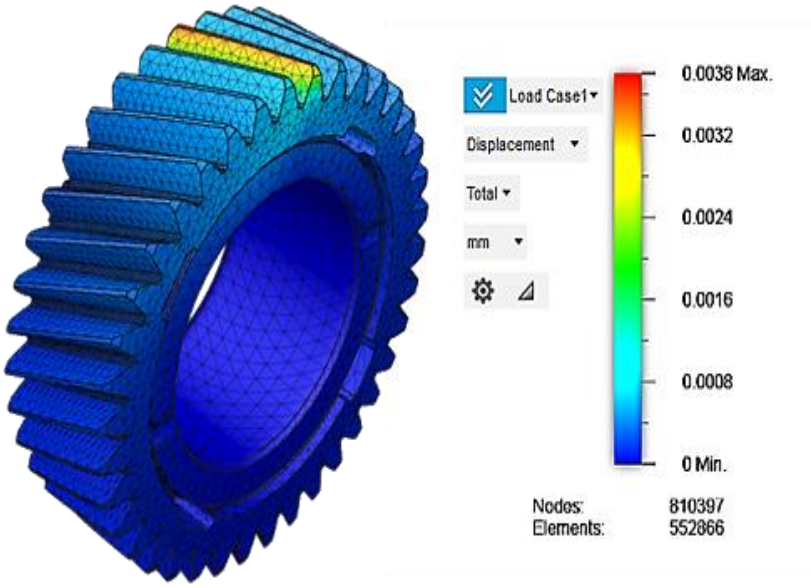

Figure 24.
Maximum displacement, valid for gear z_8, mass reduced by 4%.

Edelweiss Applied Science and Technology
ISSN: 2576-8484
Vol. 7, No. 1: 38-70, 2023
DOI: 10.55214/25768484.v7i1.333

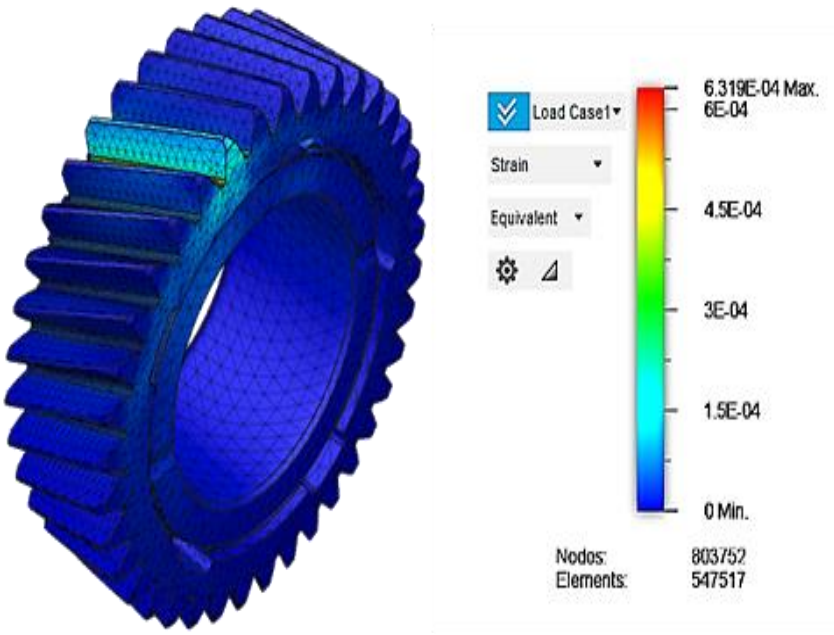

Figure 25.
Maximum equivalent strain, valid for gear z_8, mass reduced by 4%.

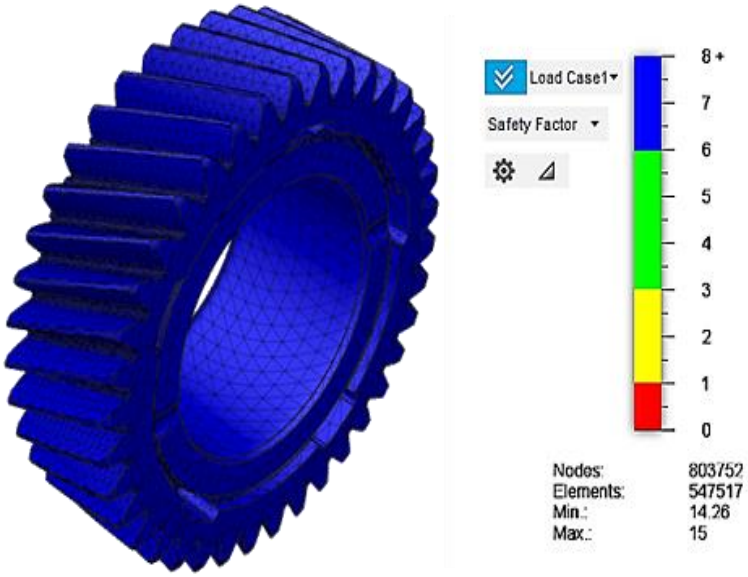

Figure 26.
Minimum safety factor, valid for gear z_8, mass reduced by 5%.

Edelweiss Applied Science and Technology
ISSN: 2576-8484
Vol. 7, No. 1: 38-70, 2023
DOI: 10.55214/25768484.v7i1.333

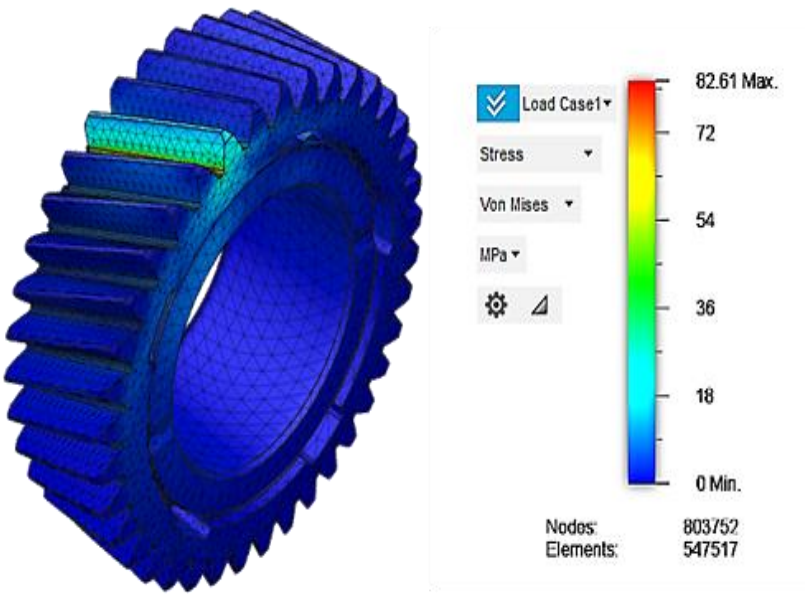

Figure 27.
Maximum Von Mises stress, valid for gear z_8, mass reduced by 5%.

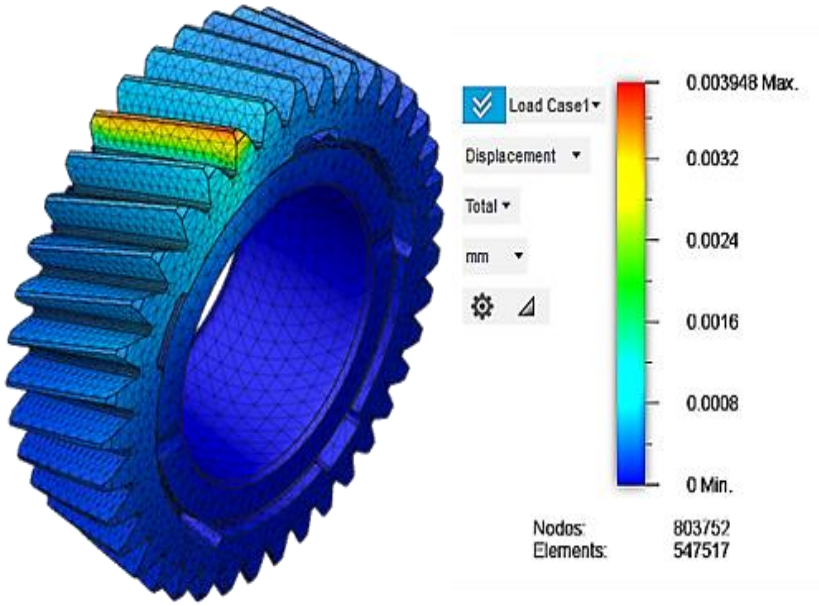

Figure 28.
Maximum displacement, valid for gear z_8, mass reduced by 5%.

Edelweiss Applied Science and Technology
ISSN: 2576-8484
Vol. 7, No. 1: 38-70, 2023
DOI: 10.55214/25768484.v7i1.333

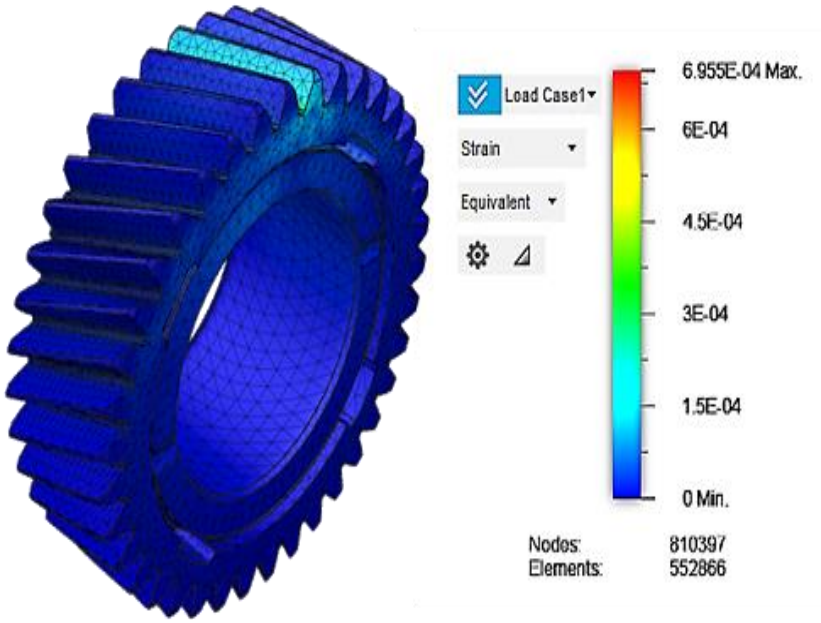

Figure 29.
Maximum equivalent strain, valid for gear z_8, mass reduced by 5%.

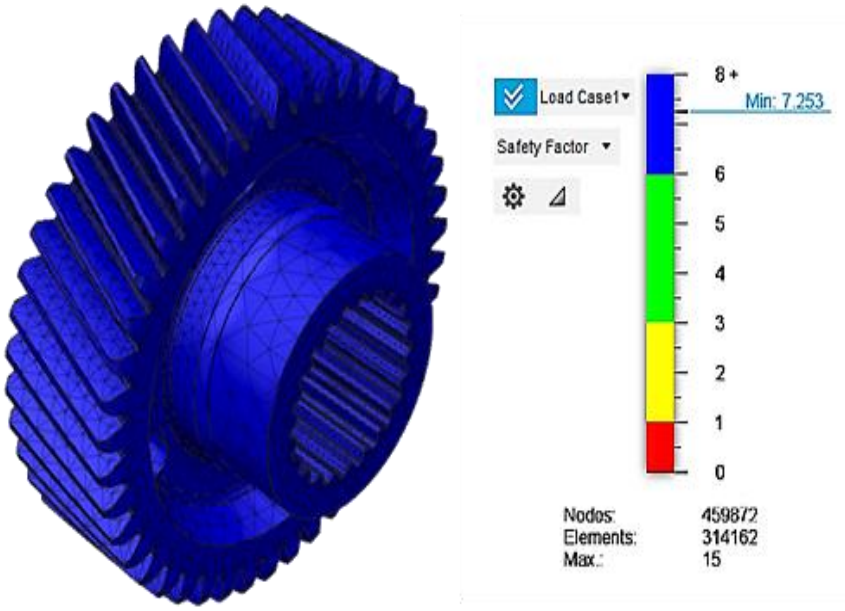

Figure 30.
Minimum safety factor, valid for gear z_9, mass reduced by 3%.

Edelweiss Applied Science and Technology
ISSN: 2576-8484
Vol. 7, No. 1: 38-70, 2023
DOI: 10.55214/25768484.v7i1.333

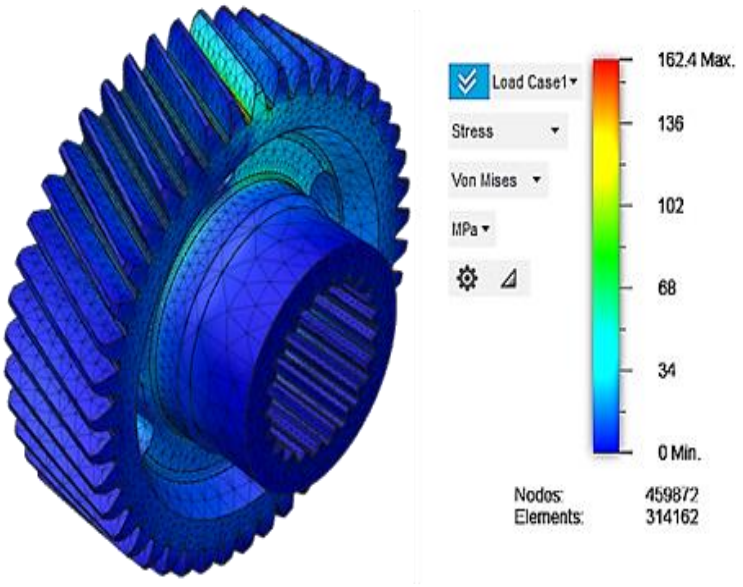

Figure 31.
Maximum Von Mises stress, valid for gear z_9, mass reduced by 3%.

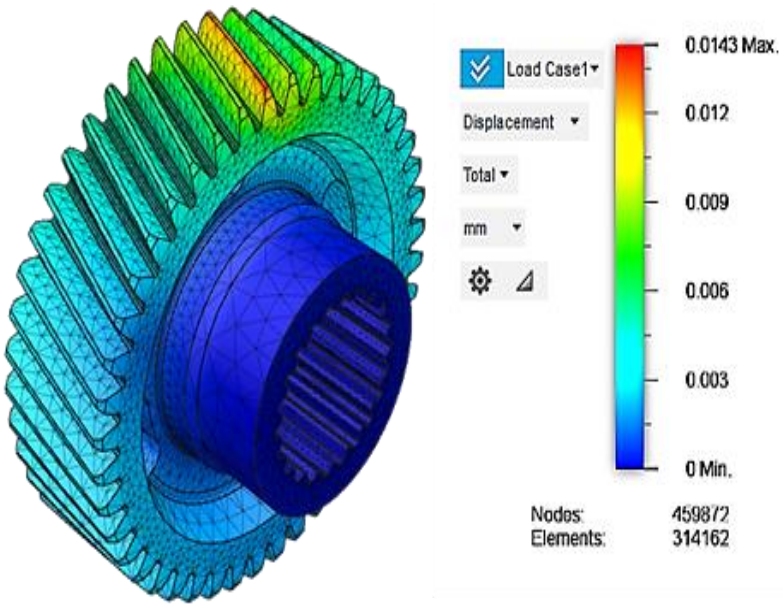

Figure 32.
Maximum displacement, valid for gear z_9, mass reduced by 3%.

Edelweiss Applied Science and Technology
ISSN: 2576-8484
Vol. 7, No. 1: 38-70, 2023
DOI: 10.55214/25768484.v7i1.333

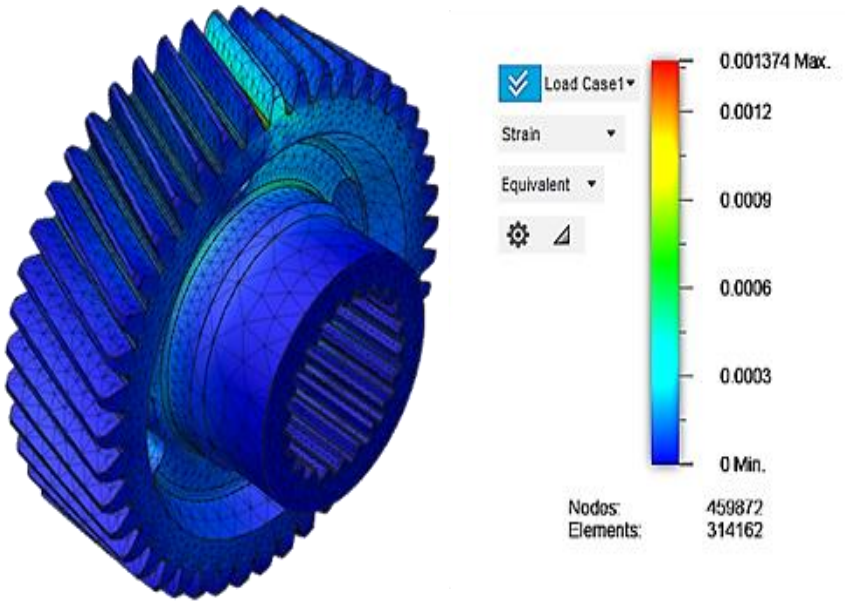

Figure 33.
Maximum equivalent strain, valid for gear z_9, mass reduced by 3%.

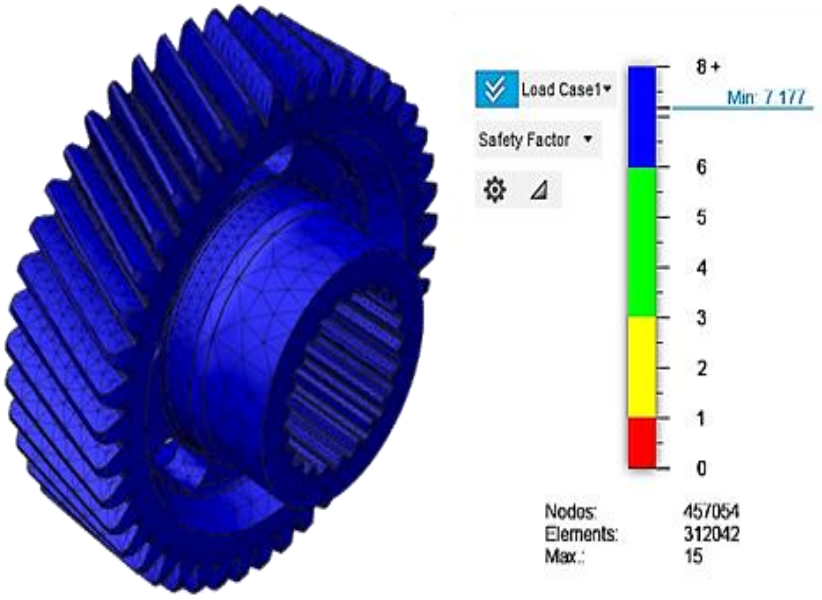

Figure 34.
Minimum safety factor, valid for gear z_9, mass reduced by 4%.

Edelweiss Applied Science and Technology
ISSN: 2576-8484
Vol. 7, No. 1: 38-70, 2023
DOI: 10.55214/25768484.v7i1.333

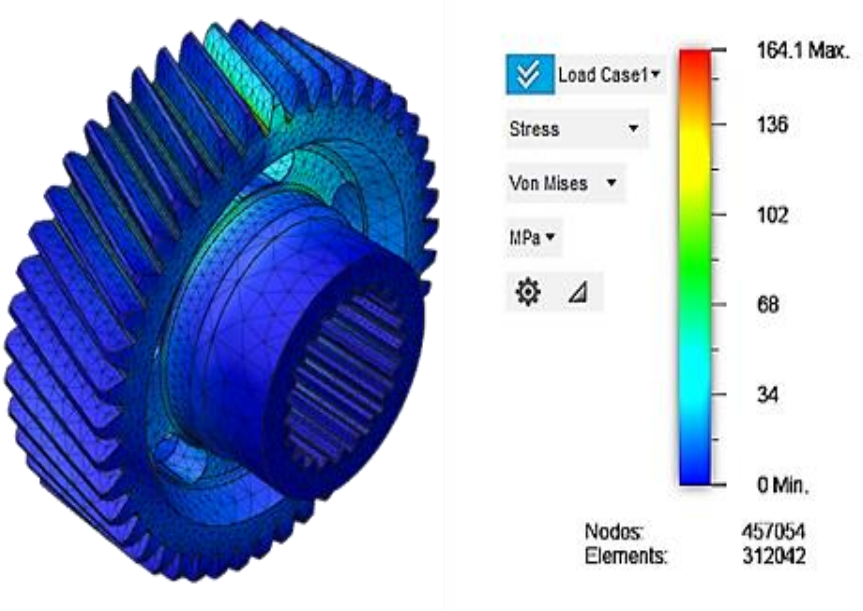

Figure 35.
Maximum Von Mises stress, valid for gear z_9, mass reduced by 4%.

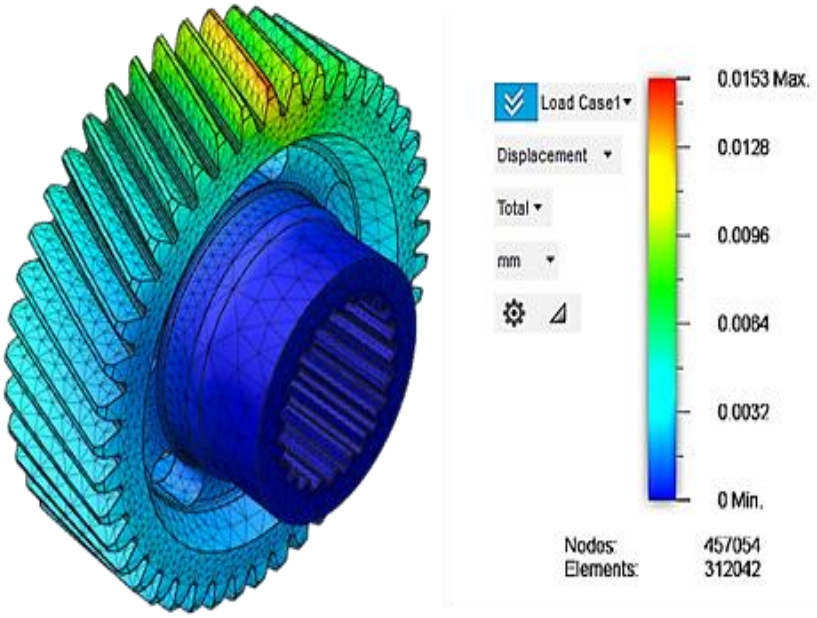

Figure 36.
Maximum displacement, valid for gear z_9, mass reduced by 4%.

Edelweiss Applied Science and Technology
ISSN: 2576-8484
Vol. 7, No. 1: 38-70, 2023
DOI: 10.55214/25768484.v7i1.333

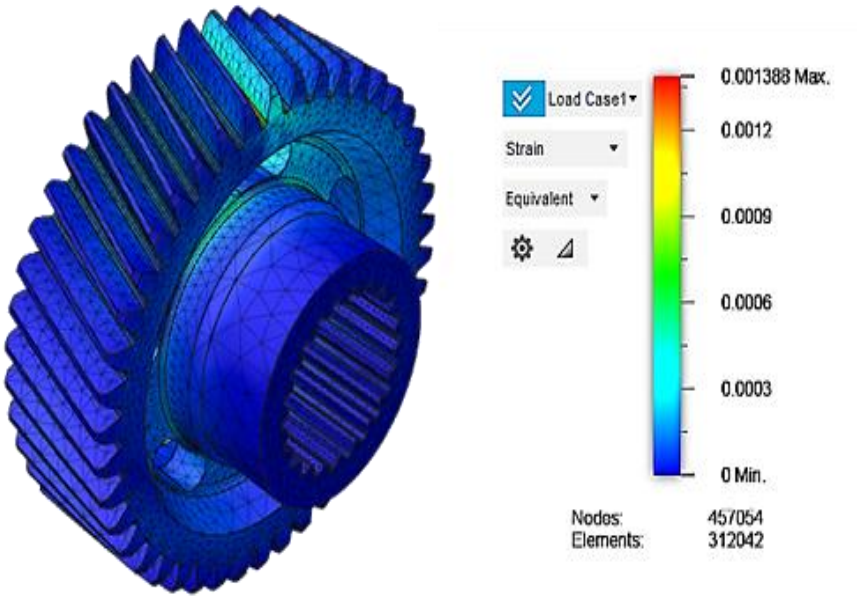

Figure 37.
Maximum equivalent strain, valid for gear z_9, mass reduced by 4%.

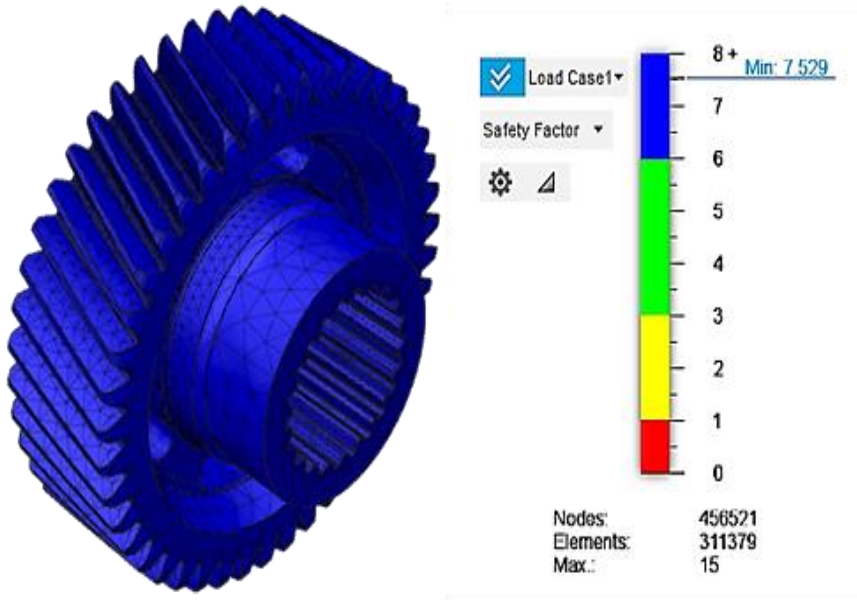

Figure 38.
Minimum safety factor, valid for gear z_9, mass reduced by 5%.

Edelweiss Applied Science and Technology
ISSN: 2576-8484
Vol. 7, No. 1: 38-70, 2023
DOI: 10.55214/25768484.v7i1.333

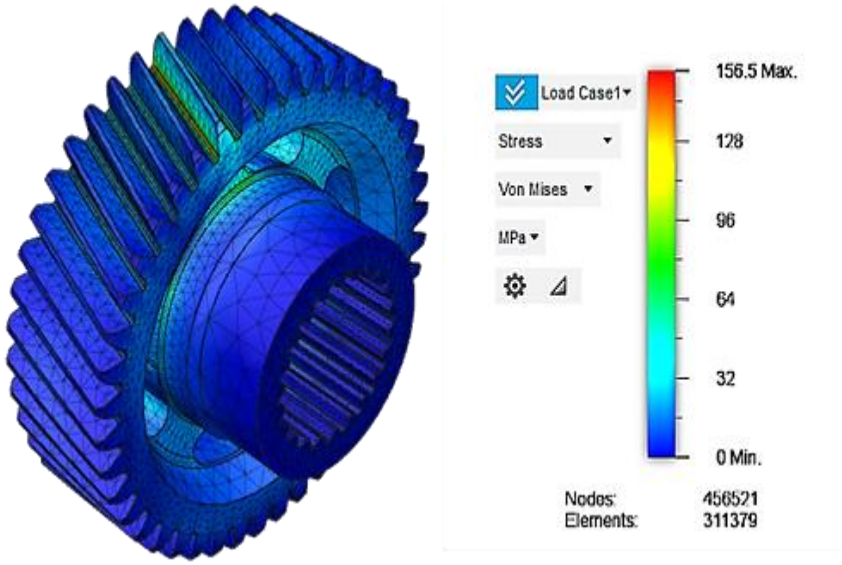

Figure 39.
Maximum Von Mises stress, valid for gear z_9, mass reduced by 5%.

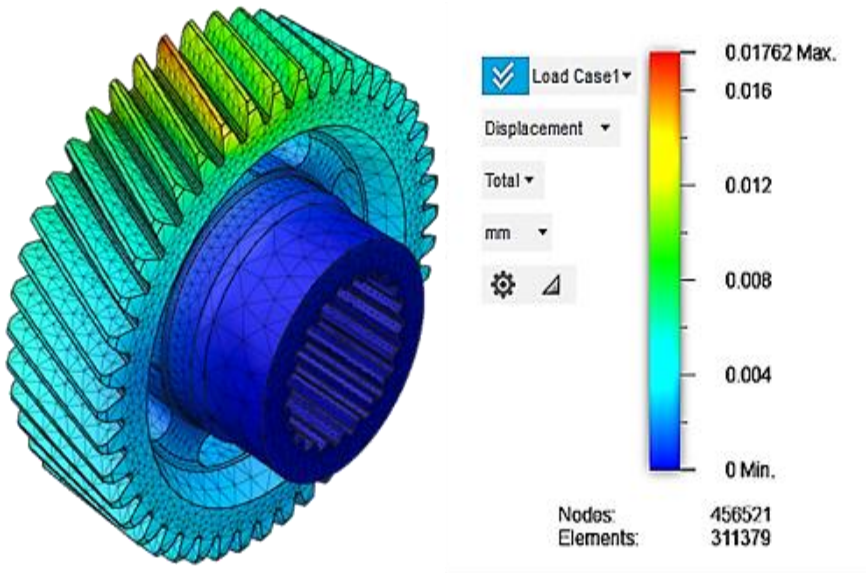

Figure 40.
Maximum displacement, valid for gear z_9, mass reduced by 5%.

Edelweiss Applied Science and Technology
ISSN: 2576-8484
Vol. 7, No. 1: 38-70, 2023
DOI: 10.55214/25768484.v7i1.333

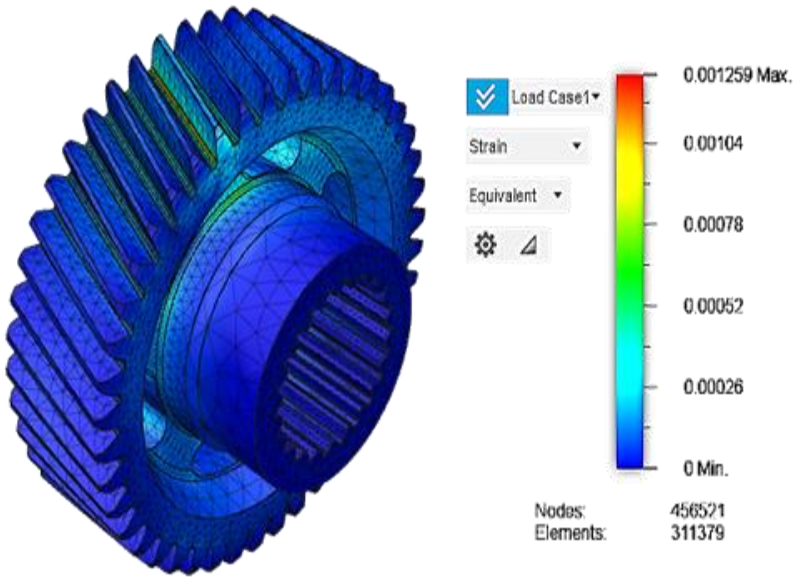

Figure 41.
Maximum equivalent strain, valid for gear z_9, mass reduced by 5%.

Scenario I of topological optimisation reduced the mass of gear z_8 by 3%, resulting in a decline in all analysed parameters, with values decreasing by 3 to 10% compared to the reference values.

Scenario II of topological optimisation brought significant improvements for all analysed parameters, with increases ranging from 1 to 3% compared to the reference values.

Scenario III of topological optimisation brought improvements for most parameters, apart from the total displacement, which increased by about 3% compared to the reference value. The minimum safety factor and the equivalent Von Mises stress improved by about 0.5%, and the equivalent strain improved significantly, by about 12%, compared to the reference value.

Scenario IV of topological optimisation did not bring significant improvements for gear z_9, except for a slight improvement in the equivalent strain, by about 0.2%, compared to the reference value. The minimum safety factor and the equivalent Von Mises stress decreased by about 0.5%, compared to the reference value, and the total displacement increased by about 9%.

Scenario V of topological optimisation did not result in any improvements for the analysed parameters, with all values declining by 1 to 17%, compared to the reference values.

Scenario VI of topological optimisation was the most advantageous scenario for gear z_9, with all analysed parameters showing improvements in the part behaviour under stress, except for the total displacement, which increased by about 35%. The minimum safety factor and the equivalent Von Mises stress improved by about 3% compared to the reference values, and the equivalent strain improved by about 9% compared to the reference value.

Figure 42 and Figure 43 show the relationship between the minimum safety factor, Min_{Saf_Fac}, and mass reduction percentage, δ_{mass}, for both analysis scenarios, with the minimum safety factor expressed in absolute values.

Edelweiss Applied Science and Technology
ISSN: 2576-8484
Vol. 7, No. 1: 38-70, 2023
DOI: 10.55214/25768484.v7i1.333

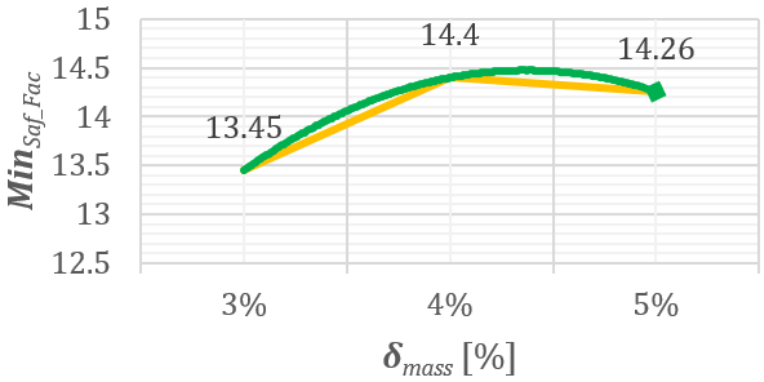

Figure 42.
Variation of the minimum safety factor, Min_{Saf_Fac} for the geared wheel z_8.

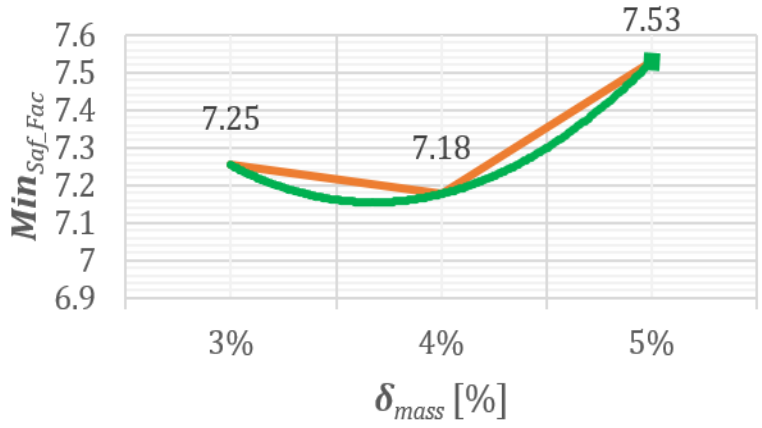

Figure 43.
Variation of the minimum safety factor, Min_{Saf_Fac} for the geared wheel z_9.

Additionally, these graphs also display the variation curve of the minimum safety factor, Min_{Saf_Fac}, specific to each analysed geared wheel, denoted as $VAR_{ABS\_j\_Min_{Saf\_Fac}}$, where j is z_8 or z_9:

$$VAR_{ABS\_z_8\_Min_{Saf\_Fac}}: Min_{Saf\_Fac} = -54.5 \cdot 10^{-2}\delta_{mass}^2 + 2.58\delta_{mass} + 11.4 \quad (1)$$

$$VAR_{ABS\_z_9\_Min_{Saf\_Fac}}: Min_{Saf\_Fac} = 21.4 \cdot 10^{-2}\delta_{mass}^2 - 71.8 \cdot 10^{-2}\delta_{mass} + 7.75 \quad (2)$$

The variation of the minimum safety factor, Min_{Saf_Fac}, in relative values to the nominal simulation scenario, as a function of mass reduction percentage, δ_{mass}, is shown in Figure 44 and Figure 45. Additionally, these figures also depict the variation curve of the minimum safety factor, Min_{Saf_Fac}, specific to each topological optimisation scenario, denoted as $VAR_{REL\_j\_Min_{Saf\_Fac}}$, where j is z_8 or z_9:

Edelweiss Applied Science and Technology
ISSN: 2576-8484
Vol. 7, No. 1: 38-70, 2023
DOI: 10.55214/25768484.v7i1.333

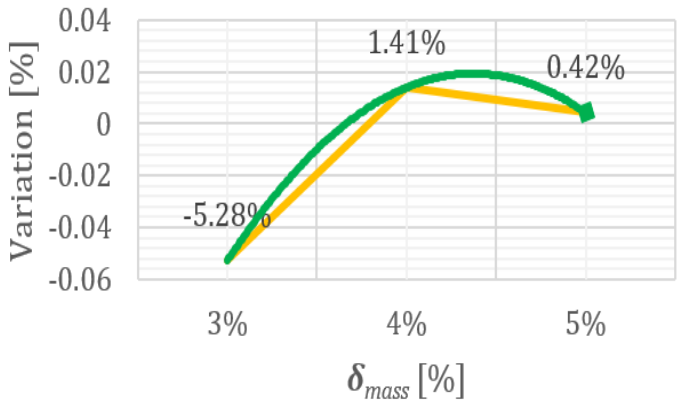

Figure 44.
Variation of the minimum safety factor, Min_{Saf_Fac} in relative values to the nominal simulation scenario, as a function of mass reduction percentage, δ_{mass}, for the geared wheel z_8.

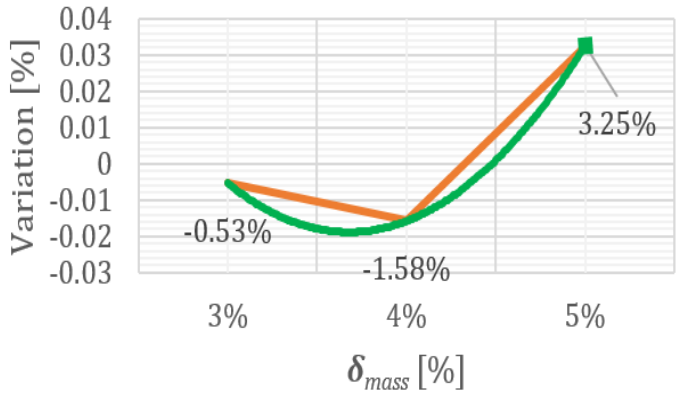

Figure 45.
Variation of the minimum safety factor, Min_{Saf_Fac} in relative values to the nominal simulation scenario, as a function of mass reduction percentage, δ_{mass}, for the geared wheel z_9.

$$VAR_{REL\_z_8\_Min_{Saf\_Fac}}: Min_{Saf\_Fac} = -3.84 \cdot 10^{-2}\delta_{mass}^2 + 18.2 \cdot 10^{-2}\delta_{mass} - 19.6 \cdot 10^{-2} \quad (3)$$

$$VAR_{REL\_z_9\_Min_{Saf\_Fac}}: Min_{Saf\_Fac} = 29.3 \cdot 10^{-2}\delta_{mass}^2 - 98.5 \cdot 10^{-2}\delta_{mass} + 6.38 \cdot 10^{-2} \quad (4)$$

The variation of the Von Mises equivalent stress, σ_{VM}, in absolute values, as a function of mass reduction percentage, δ_{mass}, is shown in Figure 46and Figure 47. Additionally, these figures also display the variation curve of the Von Mises equivalent stress, σ_{VM}, specific to each topological optimisation scenario, denoted as $VAR_{ABS\_j\_\sigma_{VM}}$, where $j$is z_8 or z_9:

$$VAR_{ABS\_z_8\_\sigma_{VM}}: \sigma_{VM} = 3.3\delta_{mass}^2 - 15.7\delta_{mass} + 99.9 \quad (5)$$

$$VAR_{ABS\_z_9\_\sigma_{VM}}: \sigma_{VM} = -4.65\delta_{mass}^2 + 15.65\delta_{mass} + 151.4 \quad (6)$$

Edelweiss Applied Science and Technology
ISSN: 2576-8484
Vol. 7, No. 1: 38-70, 2023
DOI: 10.55214/25768484.v7i1.333

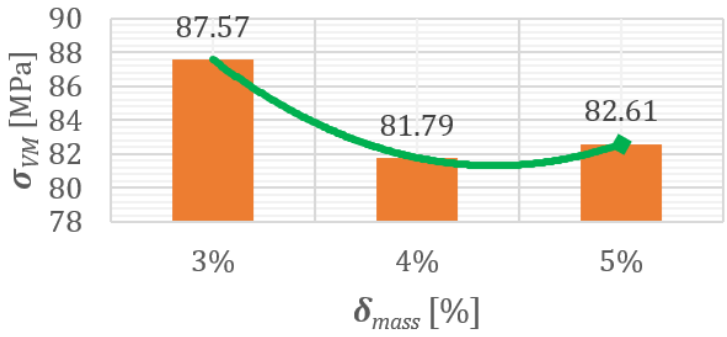

Figure 46.
Variation of the Von Mises equivalent stress, σ_{VM}, in absolute values, as a function of mass reduction percentage, δ_{mass}, for the geared wheel z_8.

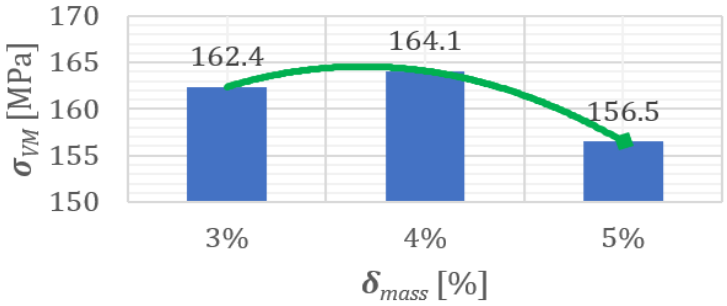

Figure 47.
Graphical representation of the variation of the Von Mises equivalent stress, σ_{VM}, in absolute values, as a function of mass reduction percentage, δ_{mass}, for the geared wheel z_9.

The variation of the Von Mises equivalent stress, σ_{VM}, in relative values to the nominal simulation scenario, as a function of mass reduction percentage, δ_{mass}, is shown in Figure 48 and Figure 49. Additionally, these figures also display the variation curve of the Von Mises equivalent stress, σ_{VM}, specific to each geared wheel, denoted as $VAR_{REL\_j\_\sigma_{VM}}$, where j is z_8 or z_9:

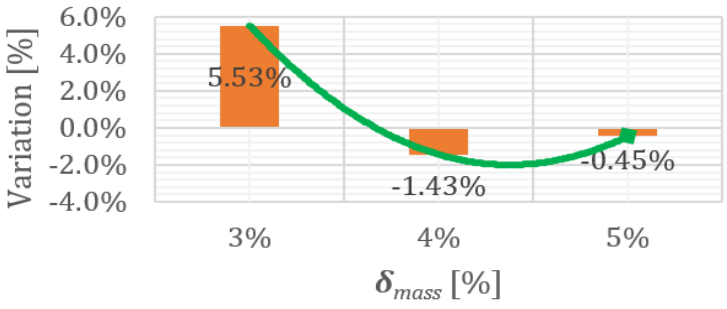

Figure 48.
Von Mises equivalent stress, σ_{VM}, in relative values to the nominal simulation scenario, as a function of mass reduction percentage, δ_{mass}, for the geared wheel z_8.

Edelweiss Applied Science and Technology
ISSN: 2576-8484
Vol. 7, No. 1: 38-70, 2023
DOI: 10.55214/25768484.v7i1.333

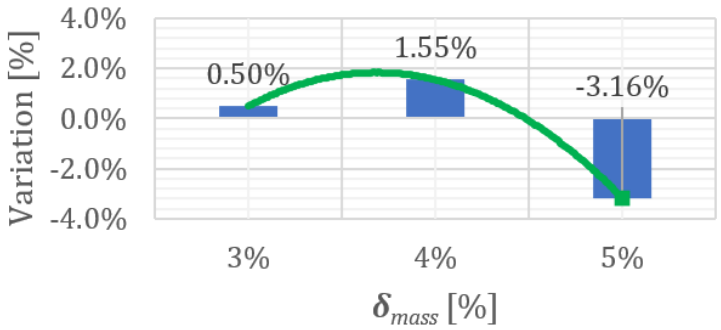

Figure 49.
Von Mises equivalent stress, σ_{VM}, in relative values to the nominal simulation scenario, as a function of mass reduction percentage, δ_{mass}, for the geared wheel z_9.

$$VAR_{REL\_z_8\_\sigma_{VM}}: \sigma_{VM} = 3.98 \cdot 10^{-2}\delta_{mass}^2 - 18.9 \cdot 10^{-2}\delta_{mass} + 20.4 \cdot 10^{-2} \quad (7)$$

$$VAR_{REL\_z_9\_\sigma_{VM}}: \sigma_{VM} = -2.88 \cdot 10^{-2}\delta_{mass}^2 + 9.68 \cdot 10^{-2}\delta_{mass} - 6.31 \cdot 10^{-2} \quad (8)$$

The variation of the maximum displacement, d, in absolute values, as a function of mass reduction percentage, δ_{mass}, is shown in Figure 50 and Figure 51. Additionally, these figures also display the variation curve of the maximum displacement, d, specific to each topological optimisation scenario, denoted as $VAR_{ABS\_j\_d}$, where j is z_8 or z_9:

$$VAR_{ABS\_z_8\_}d: d = 3 \cdot 10^{-4}\delta_{mass}^2 - 12 \cdot 10^{-4}\delta_{mass} + 52 \cdot 10^{-4} \quad (9)$$

$$VAR_{ABS\_z_9\_}d: d - 7 \cdot 10^{-4}\delta_{mass}^2 - 10^{-3}\delta_{mass} + 14.6 \cdot 10^{-3} \quad (10)$$

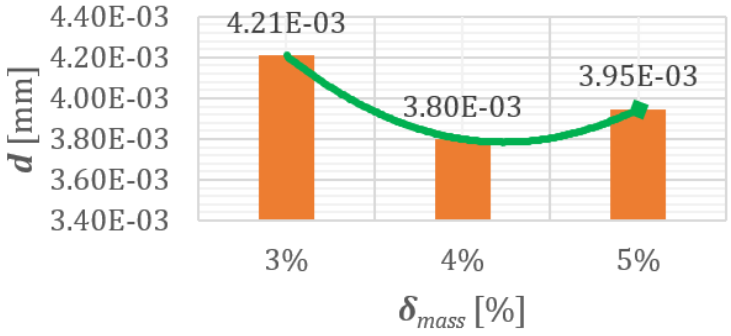

Figure 50.
Variation of the maximum displacement, d, in absolute values, as a function of mass reduction percentage, δ_{mass}, for the geared wheel z_8.

Edelweiss Applied Science and Technology
ISSN: 2576-8484
Vol. 7, No. 1: 38-70, 2023
DOI: 10.55214/25768484.v7i1.333

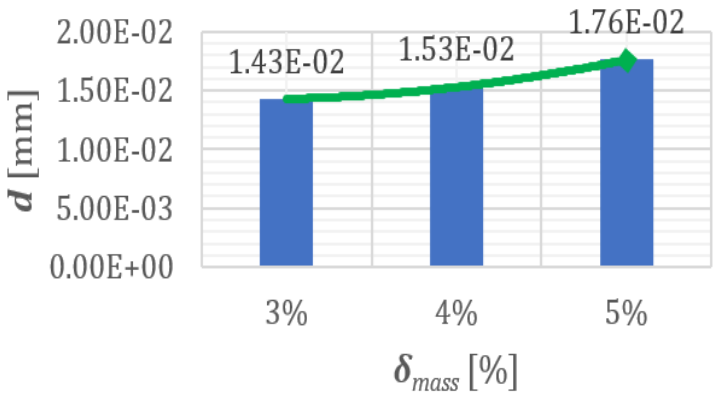

Figure 51.
Variation of the maximum displacement, d, in absolute values, as a function of mass reduction percentage, δ_{mass}, for the geared wheel z_9.

The variation of the maximum displacement, d, in relative values to the nominal simulation scenario, as a function of mass reduction percentage, δ_{mass}, is shown in Figure 52 and Figure 53. Additionally, these figures also display the variation curve of the maximum displacement, d, specific to each geared wheel, denoted as $VAR_{REL\_j\_d}$, where j is z_8 or z_9:

$$VAR_{REL\_z_8\_}d{:}d = 7.24 \cdot 10^{-2}\delta_{mass}^2 - 32.35 \cdot 10^{-2}\delta_{mass} + 34.52 \cdot 10^{-2} \quad (11)$$

$$VAR_{REL\_z_9\_}d{:}d - 50.3 \cdot 10^{-3}\delta_{mass}^2 - 74.6 \cdot 10^{-3}\delta_{mass} + 11.35 \cdot 10^{-2} (12)$$

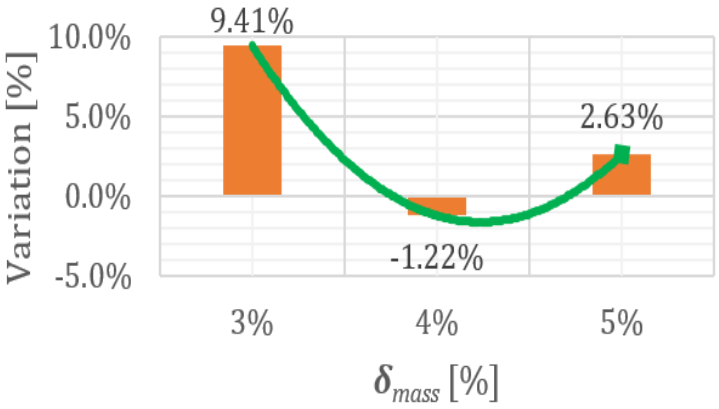

Figure 52.
Maximum displacement, d, in relative values to the nominal simulation scenario, as a function of mass reduction percentage, δ_{mass}, for the geared wheel z_8.

Edelweiss Applied Science and Technology
ISSN: 2576-8484
Vol. 7, No. 1: 38-70, 2023
DOI: 10.55214/25768484.v7i1.333

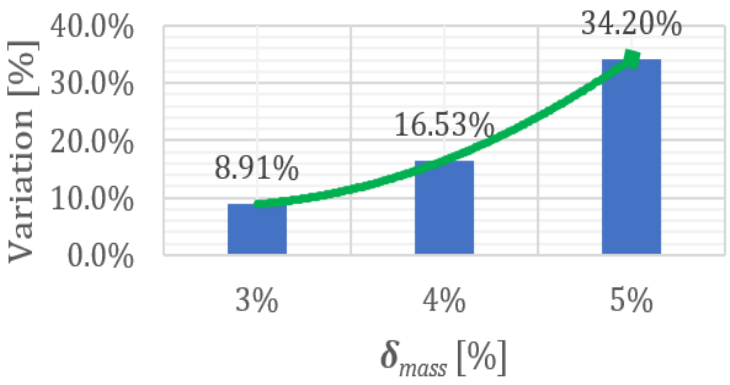

Figure 53.
Maximum displacement, d, in relative values to the nominal simulation scenario, as a function of mass reduction percentage, δ_{mass}, for the geared wheel z_9.

The variation of the maximum equivalent strain, $\boldsymbol{\varepsilon}$, in absolute values, as a function of mass reduction percentage, δ_{mass}, is shown in Figure 54 and Figure 55. Additionally, these figures also display the variation curve of the maximum equivalent strain, ε, specific to each topological optimisation scenario, denoted as $VAR_{ABS\_j\_\varepsilon}$, where j is z_8 or z_9:

$$VAR_{ABS\_z_8\_}\varepsilon: \varepsilon = -1{,}23 \cdot 10^{-5}\delta_{mass}^2 - 2.1 \cdot 10^{-6}\delta_{mass} + 7.48 \cdot 10^{-4} \quad (13)$$

$$VAR_{ABS\_z_9\_}\varepsilon: \varepsilon = -7.15 \cdot 10^{-5}\delta_{mass}^2 + 2.28 \cdot 10^{-4}\delta_{mass} + 1.21 \cdot 10^{-3} \quad (14)$$

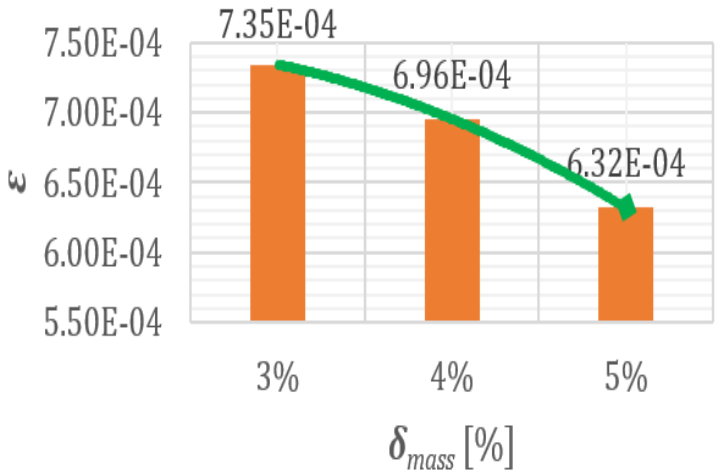

Figure 54.
Variation of the maximum equivalent strain, ε, in absolute values, as a function of mass reduction percentage, δ_{mass}, for the geared wheel z_8.

Edelweiss Applied Science and Technology
ISSN: 2576-8484
Vol. 7, No. 1: 38-70, 2023
DOI: 10.55214/25768484.v7i1.333

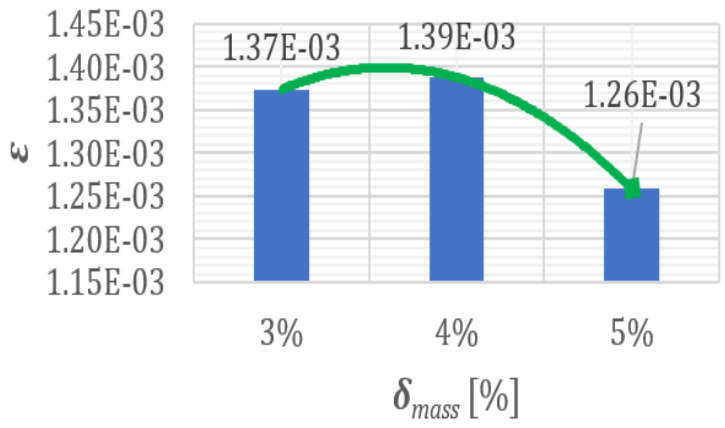

Figure 55.
Variation of the maximum equivalent strain, ε, in absolute values, as a function of mass reduction percentage, δ_{mass}, for the geared wheel z_9.

The variation of the maximum equivalent strain, ε, in relative values to the nominal simulation scenario, as a function of mass reduction percentage, δ_{mass}, is shown in Figure 56 and Figure 57. Additionally, these figures also display the variation curve of the maximum equivalent strain, ε, specific to each geared wheel, denoted as $VAR_{REL\_j\_\varepsilon}$, where j is z_8 or z_9:

$$VAR_{REL\_z_8\_}\varepsilon{:}\varepsilon = -17.3 \cdot 10^{-3}\delta_{mass}^2 - 2.9 \cdot 10^{-3}\delta_{mass} + 50.9 \cdot 10^{-3} \quad (15)$$

$$VAR_{REL\_z_9\_}\varepsilon{:}\varepsilon = -51.9 \cdot 10^{-3}\delta_{mass}^2 + 16.59 \cdot 10^{-2}\delta_{mass} - 11.62 \cdot 10^{-2} \quad (16)$$

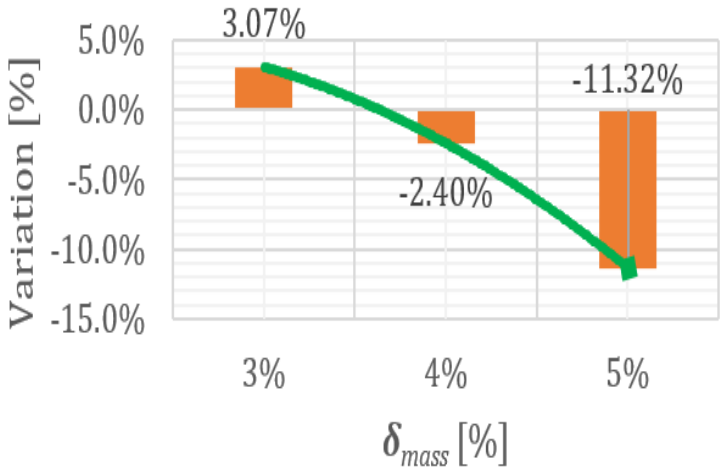

Figure 56.
Variation of the maximum equivalent strain, ε, in relative values to the nominal simulation scenario, as a function of mass reduction percentage, δ_{mass}, for the geared wheel z_8.

Edelweiss Applied Science and Technology
ISSN: 2576-8484
Vol. 7, No. 1: 38-70, 2023
DOI: 10.55214/25768484.v7i1.333

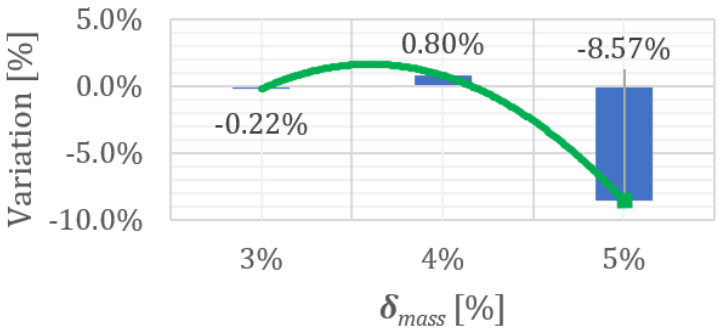

Figure 57.
Variation of the maximum equivalent strain, ε, in relative values to the nominal simulation scenario, as a function of mass reduction percentage, δ_{mass}, for the geared wheel z_9.

5. Conclusions

Topology optimisation Scenario I, where the mass of the geared wheel z_8 is reduced by 3%, does not provide any additional benefits beyond the mass reduction itself.

Topology optimisation Scenario II, where the mass of the geared wheel z_8 is reduced by 4%, is the most advantageous optimisation scenario for this wheel, as it improves all analysed parameters.

Topology optimisation Scenario III, where the mass of the geared wheel z_8 is reduced by 5%, improving most analysed parameters. The 5% mass reduction must also be justified from an economic and technical standpoint, and the risk/gain ratio must be calculated in the event of optimisation, as a 5% reduction in mass leads to approximately a 3% increase in total displacement.

Topology optimisation beyond the mass reduction itself, Scenario IV, which reduces the geared wheels z_9 mass by 3%, does not offer any additional advantages.

Topology optimisation Scenario V, where the mass of the geared wheel z_9 is reduced by 4%, has a negative impact on all analysed parameters, with values ranging from approximately 1% to 17%. This makes it the least favourable optimisation scenario.

Topology optimisation Scenario VI, where the mass of the geared wheel z_9 is reduced by 5%, improves most of the analysed parameters. From a technical standpoint, this optimisation scenario is plausible, but a risk-gain analysis should be conducted. In the event of a possible optimisation, a gain of 5% mass reduction would need a proper justification, as it would lead to an approximately 35% increase in total displacement.

One potential benefit of using topology optimisation to improve the design of a gear wheel pair is that it can lead to a more efficient and lightweight design. This is because the optimisation process can identify the minimum amount of material needed to meet the required strength and stiffness requirements without any excess material being used. This can result in a gear pair that is lighter in weight, which can help reduce the overall mass of the drivetrain and improve the vehicle's fuel efficiency.

In addition to improving the weight of the gears, topology optimisation can also be used to improve their durability and performance. By optimising the layout of the gear material, it is possible to create a design that can withstand higher loads and deformations, which can lead to improved transmission efficiency and reduced wear on the gears. This is particularly important in high-performance vehicles, where the drivetrain is subjected to greater loads and stresses due to the higher speeds and acceleration levels.

One potential limitation of using topology optimisation to improve the design of a gear wheel pair is that it can be a time-consuming and computationally intensive process. The optimisation algorithms

Edelweiss Applied Science and Technology
ISSN: 2576-8484
Vol. 7, No. 1: 38-70, 2023
DOI: 10.55214/25768484.v7i1.333

must be run numerous times to find the optimal layout of the gear material, which can take a significant amount of time and resources. In addition, the accuracy of the optimisation results may be limited by the quality and resolution of the finite element model being used.

Despite these limitations, the use of topology optimisation can provide significant benefits in the design of a gearwheel pair. By identifying the optimal layout of the gear material, it is possible to create a design that is stronger, more efficient, and longer-lasting, which can lead to improved transmission performance and overall vehicle performance. As such, the use of topology optimisation is likely to become increasingly important in the design of automotive gears and other drivetrain components in the future.

The authors have concluded that topology optimisation scenarios III and VI show the highest degree of relevance for further design optimisation based on the previously mentioned results.

Funding:
This study received no specific financial support.

Institutional Review Board Statement:
Not applicable.

Transparency:
The authors confirm that the manuscript is an honest, accurate, and transparent account of the study; that no vital features of the study have been omitted; and that any discrepancies from the study as planned have been explained. This study followed all ethical practices during writing.

Competing Interests:
The authors declare that they have no competing interests.

Authors' Contributions:
All authors contributed equally to the conception and design of the study. All authors have read and agreed to the published version of the manuscript.

References
[1] S. G. Barbieri, M. Giacopini, V. Mangeruga, and S. Mantovani, "A design based on topology optimization techniques for an additive manufactured high-performance engine piston," presented at the Procedia Manufacturing 27th International Conference on Flexible Automation and Intelligent Manufacturing, FAIM 2017, Modena, Italy, June 2017, Volume 11, pp 641-649, 2017.

[2] P. Barreiro, A. Bronner, J. Hoffmeister, and J. Hermes, "New improvement opportunities through applying topology optimization combined with 3D printing to the construction of gearbox housings," *Forschung im Ingenieurwesen*, vol. 3, no. 83, pp. 669-681, 2019.

[3] M. P. Bendsøe and O. Sigmung, *Topology optimization theory, methods and applications*, 2nd ed. Berlin: Springer Publishing, 2004.

[4] G. Fraţilă and M. Untaru, *Calculation and construction of automobiles (in Romanian)*. Bucharest: Didactics and Pedagogy Publishing House, 1982.

[5] M. Gaidur *et al.*, "Improving brake efficiency by optimizing the design of a car brake caliper," In IOP Conference Series: Materials Science and Engineering (Vol. 997, No. 1, p. 012116). IOP Publishing, 2020.

[6] M. Gaidur, I. Pascal, E. Rakosi, T. Ulian, S. Talif, and G. Manolache, "Analytical study regarding topological optimization of an internal combustion engine cylinder block," presented at the IOP Conference Series –Materials Science and Engineering, 2022.

[7] M. Gaidur, P. Ionut, R. Edward, T. Ulian, S. Talif, and G. Manolache, "Contributions towards improving the displacement and strain responses of an internal combustion engine piston through topology optimization," In IOP Conference Series: Materials Science and Engineering (Vol. 1220, No. 1, p. 012020). IOP Publishing, 2022.

[8] D. Vlah, R. Žavbi, and N. Vukašinović, "Evaluation of topology optimization and generative design tools as support for conceptual design," in In Proceedings of the Design Society: DESIGN Conference (Vol. 1, pp. 451-460). Cambridge University Press, 2020.

[9] J. P. Wang, G. Liu, S. Chang, and L. Y. Wu, "Topology optimization of gearbox to reduce radiated noise," in *Proceedings of the ASME 2015 International Design Engineering Technical Conferences & Computers and Information in Engineering Conference IDETC/CIE 2015, Boston - USA*, 2015.

[10] S. Xu, J. Liu, B. Zou, Q. Li, and Y. Ma, "Stress constrained multi-material topology optimization with the ordered SIMP method," *Computer Methods in Applied Mechanics and Engineering*, vol. 373, p. 113453, 2021.

[11] S. Zhang, A. L. Gain, and J. A. Norato, "Adaptive mesh refinement for topology optimization with discrete geometric components," *Computer Methods in Applied Mechanics and Engineering*, vol. 364, p. 112930, 2020.

[12] W. Zheng, Y. Wang, Y. Zheng, and D. Da, "Efficient topology optimization based on DOF reduction and convergence acceleration methods," *Advances in Engineering Software*, vol. 149, p. 102890, 2020.

[13] B. Zhu *et al.*, "Design of compliant mechanisms using continuum topology optimization: A review," *Mechanism and Machine Theory*, vol. 143, p. 103622, 2020.

[14] Z. H. U. Jihong, Z. H. O. U. Han, W. A. N. G. Chuang, Z. H. O. U. Lu, Y. U. A. N. Shangqin, and W. Zhang, "A review of topology optimization for additive manufacturing: Status and challenges," *Chinese Journal of Aeronautics*, vol. 34, no. 1, pp. 91-110, 2021.

[15] ISO 54, "ISO 54: 1996 Cylindrical gears for general engineering and for heavy duty - Modules," Retrieved: https://www.iso.org/standard/22644.html. [Accessed 2023], 1996.

[16] DIN EN 10250, "Open die steel forgings for general engineering purposes - part 3: Alloy special steels," Retrieved: https://www.din.de/en/getting-involved/standards-committees/fes/publications/wdc-beuth:din21:345157069. [Accessed 2022], 2022.

Edelweiss Applied Science and Technology
ISSN: 2576-8484
Vol. 7, No. 1: 38-70, 2023
DOI: 10.55214/25768484.v7i1.333